Chinese Journal of Catalysis 42 (2021) 388–395

available at www.sciencedirect.com

ScienceDirect

journal homepage: www.elsevier.com/locate/chnjc

Article

Highly dispersed boron-nitride/CuO_x-supported Au nanoparticles for catalytic CO oxidation at low temperatures

Fan Wu, Lei He, Wen-Cui Li, Rao Lu, Yang Wang, An-Hui Lu *

State Key Laboratory of Fine Chemicals, Liaoning Key Laboratory for Catalytic Conversion of Carbon Resources, School of Chemical Engineering, Dalian University of Technology, Dalian 116024, Liaoning, China

ARTICLE INFO

Article history:
Received 20 April 2020
Accepted 26 May 2020
Published 5 March 2021

Keywords:
Boron nitride
Au catalyst
CO oxidation
CuO
Electron transfer

ABSTRACT

Supported-Au catalysts show excellent activity in CO oxidation, where the nature of the support has a significant impact on catalytic activity. In this work, a hexagonal boron nitride (BN) support with a high surface area and adequately exposed edges was obtained by the ball-milling technique. Thereafter, impregnation of the BN support with $Cu(NO_3)_2$ followed by calcination under air at 400 °C yielded a CuO-modified support. After Au loading, the obtained Au-CuO_x/BN catalyst exhibited high CO oxidation activity at low temperatures with a 50% CO conversion temperature ($T_{50\%}$) of 25 °C and a complete CO conversion temperature ($T_{100\%}$) of 80 °C, well within the operational temperature range of proton exchange membrane fuel cells. However, the CO oxidation activity of Au/BN, prepared without CuO_x for comparison, was found to be relatively low. Our study reveals that BN alone disperses both Cu and Au nanoparticles well. However, Au nanoparticles on the surface of BN in the absence of CuO species tend to aggregate upon CO oxidation reactions. Conversely, Au nanoparticles supported on the surface of CuO-modified BN remain small with an average size of ~2.0 nm before and after CO oxidation. Moreover, electron transfer between Au and Cu species possibly favors the stabilization of highly dispersed Au nanoparticles on the BN surface and also enhances CO adsorption. Thus, our results demonstrate that thermally stable and conductive CuO-modified BN is an excellent support for the preparation of highly dispersed and stable Au catalysts.

1. Introduction

CO oxidation at low temperatures (<200 °C) has been extensively studied owing to its potential practical applications and fundamental importance as a prototypical oxidation reaction for probing the activities and mechanistic details of novel catalysts. Supported-Au catalysts have attracted considerable attention and are generally accepted as the most active catalysts for CO oxidation [1,2]. Many factors can affect the activity of supported-Au catalysts, such as Au particle size, the nature of the support [3,4], and the presence of additional promoters [5–7]. Notably, varying the support material can significantly influence the catalytic performance of Au in this reaction system as different support materials exhibit different metal-support interactions [8], oxygen activation abilities [9,10], and even surface functional groups [11].

Generally, reducible oxides such as CeO_2 and TiO_2 are used for the immobilization of Au nanoparticles owing to their strong metal-support interactions [12–14]. This type of support is also beneficial for oxygen activation, consequently promoting

* Corresponding author. Tel: +86-411-84986112; E-mail: anhuilu@dlut.edu.cn
This work was supported by the State Key Program of the National Natural Science Foundation of China (21733002), Joint Sino-German Research Project (21761132011), and the Cheung Kong Scholars Program of China (T2015036).
DOI: 10.1016/S1872-2067(20)63669-5 | http://www.sciencedirect.com/science/journal/18722067 | Chin. J. Catal., Vol. 42, No. 3, March 2021

the activity of Au catalysts in CO oxidation. Non-reducible oxides that have large surface areas and are rich in defects, such as Al_2O_3, are also considered to be excellent support materials for Au catalysts and to enhance CO oxidation activity [15,16]. Furthermore, the addition of transition-metal or metal oxides can enhance the activity of Au catalysts by adjusting the electronic properties of the Au and promoting oxygen activation during the reaction [17,18]. Nevertheless, the mechanisms by which reducible and non-reducible oxides influence the catalytic performances of Au catalysts remain unclear and sometimes controversial owing to the coexistence of electronic and geometric effects in one support.

Since the discovery of its high activity and selectivity in the oxidative dehydrogenation of propane [19–21], two-dimensionally structured, thermally stable, and conductive boron nitride (BN) has attracted increasing attention as a novel active catalytic material. Moreover, spherical BN has been demonstrated as an excellent support for Au-Cu alloy nanoparticles, showing high activity in the selective oxidation of ethanol [22]. Compared to bulk BN, nanosized BN has a larger exposed surface and edges that allow the high dispersion of metal particles on its external surface defects, thus facilitating fast kinetic transfer [23]. Furthermore, the non-reducibility of BN and its relatively weak interactions with active metallic species make it easier to determine the origin of Au-catalyst activity in CO oxidation. In addition, when considering the exothermic nature of CO oxidation, the use of BN, which exhibits high thermal conductivity, may minimize the formation of reaction hot spots, making low temperature activity more reliable.

Accordingly, in this study, we used BN as a support material for the preparation of novel Au catalysts for CO oxidation at low temperatures. Furthermore, a recent study demonstrated a synergistic interaction between Au and Cu species [24] that may help to keep Au nanoparticles small and stable. Therefore, CuO was used as an additive, thus affording Au-CuO_x/BN catalysts. The optimum catalyst exhibited high activity, with a $T_{50\%}$ (50% CO conversion temperature) value of 25 °C and a $T_{100\%}$ (100% CO conversion temperature) value of 80 °C, meeting the operational temperature requirements of catalysts for proton exchange membrane fuel cells. The catalyst was characterized by various means in order to reveal the roles of the BN support and metal species in the catalytic reaction.

2. Experimental

2.1. Preparation of BN supports

Commercial hexagonal BN (Aladdin) was processed by planetary ball-milling (QM-3SP04) at 400 rpm for 4 h and then washed for 2 h with deionized water at 80 °C. Subsequently, the wet samples were suction-filtered and dried in an oven at 50 °C overnight to obtain the ball-milled BN supports.

2.2. Preparation of Au-CuO_x/BN catalysts

The BN support was first incipiently impregnated using $Cu(NO_3)_2$ aqueous solution at a theoretical CuO/BN mass ratio of 0.03 (3 wt%). Then, the sample was maintained at room temperature for 2 h and dried at 50 °C for 12 h. Finally, the sample was calcined at 400 °C for 2 h in air to obtain CuO/BN.

The Au-CuO_x/BN catalyst was prepared by a typical deposition-precipitation method at a theoretical Au/BN mass ratio of 0.03 (3 wt%). Typically, a $HAuCl_4$ solution was added dropwise to an aqueous suspension of CuO/BN at room temperature. The pH of the mixture was adjusted to 8–9 using $(NH_4)_2CO_3$ solution and the resulting solution was kept at 60 °C for 2 h. The products were then washed four times with deionized water and once with alcohol followed by centrifugal separation and drying under vacuum. Subsequently, the powder was heated to 250 °C at a heating rate of 5 °C/min and this temperature was maintained for 2 h under an oxygen atmosphere. The obtained catalysts are termed Au-CuO_x/BN. Using a theoretical Au/BN mass ratio of 0.01, another sample (1Au-CuO_x/BN) was obtained. For comparison, Au nanoparticles were supported on the same batch of BN using the above-mentioned preparation method, and the resulting catalyst is termed Au/BN.

2.3. Catalytic activity

Catalytic activity was evaluated using a fixed-bed quartz U-tube reactor using 50 mg catalyst diluted with 300 mg quartz sand (40–60 mesh). Mixtures of liquid N_2 and isopropanol at different ratios were prepared and stored in Dewar bottles, with which cold traps with temperatures of −20 and −10 °C were made. A mixture of ice and water was used to prepare a 0 °C cold trap. A thermocouple was used to monitor the temperature of the mixture during the reaction. Constant temperatures of 20 °C and above were achieved by a temperature controller connected to an electric heating furnace coupled with a thermocouple. Another thermocouple with a quartz sleeve fixed above the catalyst bed at a distance of <1 mm was used to monitor the temperature of the catalyst bed. The temperature of the catalyst bed was taken as the reaction temperature. The program heating rate was 1 °C/min. For the reaction gas, the total flow rate was 67 mL/min and the composition was 1% CO, 20% O_2, and 79% N_2. The composition of the effluent gas was analyzed using an online GC-7890 gas chromatographer (Techcomp) equipped with a thermal conductivity detector and a 5-Å molecular sieve column. The temperatures at which 50% and 100% CO conversions were achieved are termed $T_{50\%}$ and $T_{100\%}$, respectively.

2.4. Catalyst characterization

Powder X-ray diffraction (XRD) measurements were performed on a PANalytical X'Pert3 powder diffractometer using Cu K_α radiation (λ = 0.15406 nm). Diffraction patterns were collected with Cu K_α radiation (40 kV, 40 mA) over the 2θ range 10°–90°.

The actual loadings of Au and Cu in the catalysts were measured by inductively coupled plasma mass spectrometry (ICP-MS, PerkinElmer). Nitrogen adsorption-desorption isotherms were obtained with a Micromeritics TriStar 3000 adsorption analyzer. Before the measurements, all the samples

were degassed at 200 °C for 4 h, then nitrogen adsorption and desorption analyses were performed at liquid-nitrogen temperature (−196 °C). The specific surface areas (A_{BET}) were calculated from the adsorption data in the relative pressure range 0.053–0.3 using the Brunauer-Emmett-Teller (BET) method.

The morphology of the ball-milled BN was investigated using scanning electron microscopy (SEM, Hitachi SU8220) at 20 kV. Transmission electron microscopy (TEM, TECNAI F30) images were recorded at an accelerating voltage of 300 kV by dispersing ground powders in ethanol and then onto holey carbon films supported on Cu grids. High-angle annular dark field scanning transmission electron microscopy (HAADF-STEM) and energy dispersive X-ray spectroscopy (EDS) elemental mapping were conducted on a JEM-2100 F microscope.

Hydrogen temperature-programmed reduction (H_2-TPR) analyses were performed on a Micromeritics Autochem II 2920 apparatus. The samples were first dehydrated at 150 °C for 30 min under a He atmosphere. After cooling down to 50 °C, the samples were heated to 300 °C at a ramp rate of 10 °C/min in 8% H_2/Ar flow.

A Thermo Nicolet 6700 Fourier-transform infrared (FT-IR) spectrometer was used to record the FT-IR spectra of the samples. The sample was mixed with potassium bromide and compressed, then scanned directly at room temperature. Scans were performed 64 times with a resolution of 4 cm^{-1} in the wavenumber range 640–4000 cm^{-1}. Diffuse reflectance infrared Fourier transform (DRIFT) spectra were recorded on a Bruker 70V spectrometer with an *in situ* reaction cell (HARRICK) and a mercury cadmium telluride detector cooled with liquid N_2. The unpretreated samples were heated in an *in situ* reaction cell to 250 °C for 2 h under oxygen flow then cooled to 30 °C in a N_2 atmosphere to collect the background spectrum. Thereafter, 5% CO/N_2 was fed for 20 min. Subsequently, the spectra were collected until no change in the adsorption band intensities in flowing N_2 was observed.

X-ray photoelectron spectroscopy (XPS) analysis was carried out with a Thermo VG ESCALAB 250 Microprobe instrument using Al K_α radiation as the X-ray source. The binding energies of the elements were calibrated with reference to the C 1*s* peak for adventitious carbon at 284.6 eV. All samples were pretreated at 250 °C for 2 h under oxygen atmosphere, sealed, and stored in vials before XPS measurements.

3. Results and discussion

Compared to commercial BN, the ball-milled BN exhibits lower crystallinity (Fig. S1(a)), higher specific surface area (Fig. S1(b), Table S1), and more abundant surface functional groups (Fig. S2). Ball-milling is a high-energy process that is known to break down crystalline *h*-BN and create irregular layered stacks and surface defects [25]. These exposed defects are unstable and readily react with moisture, thereby forming B–OH and $–NH_2$ groups. In this study, ball-milled BN was used as a catalyst support.

TEM and SEM measurements were used to observe the morphologies of the as-synthesized support and catalysts. From the SEM images (Fig. S3(a)), the ball-milled BN modified with Cu species shows closely packed sheet-like structures. Figure S3(b)–(f) shows the microstructure of the CuO/BN catalyst. It can be seen that Cu species are finely distributed on the surface and especially the edges of the ball-milled BN. From the TEM images of the fresh Au/BN catalyst, the average size of the Au nanoparticles is ~2.8 nm, and several large Au particles (>5 nm) can be observed (Fig. 1(a), (c); Fig. S4(a), (c)). For the Au-CuO_x/BN catalyst, the Au nanoparticles are well dispersed with an average size of ~2.0 nm (Fig. 1(b), (d); Fig. S4(b), (d)), demonstrating that pre-modification of BN with CuO effectively maintains the Au nanoparticles at smaller sizes and improves their dispersion. According to the elemental mapping results for the Au-CuO_x/BN catalyst (Fig. S5), Cu and oxygen are mainly distributed over the edges of the ball-milled BN and the Au nanoparticles are coordinated with the Cu and oxygen. These results indicate that the functional groups and/or defects on the ball-milled BN may immobilize the CuO, which then further stabilize the Au nanoparticles.

The XRD patterns of the support and catalysts are shown in Fig. 2(a). For the ball-milled BN, there are six peaks at 2θ = 26.7°, 41.6°, 43.9°, 55.1°, 75.9°, and 82.1°, attributable to hexagonal BN (ICDD 01-073-2095). After loading with Cu, no peaks for Cu species are detected, which may be due to their high dispersion. After loading with Au, very weak and broad peaks representing Au can be observed for both Au/BN and Au-CuO_x/BN catalysts, indicating highly dispersed Au species with small particle sizes. The porosities of the BN and CuO/BN structures were analyzed by N_2 sorption (Table S1). The specific surface areas of BN and CuO/BN were determined to be 98 and 57 m^2/g and the corresponding pore size distributions are centered at 12.4 and 25.5 nm, which indicates the presence of mainly stacking mesopores.

The catalytic performances of BN, Au/BN, CuO/BN, and Au-CuO_x/BN for CO oxidation were investigated. As shown in Fig. 2(b), Au/BN shows negligible activity while CuO/BN exhibits very low catalytic performance. In the low-temperature

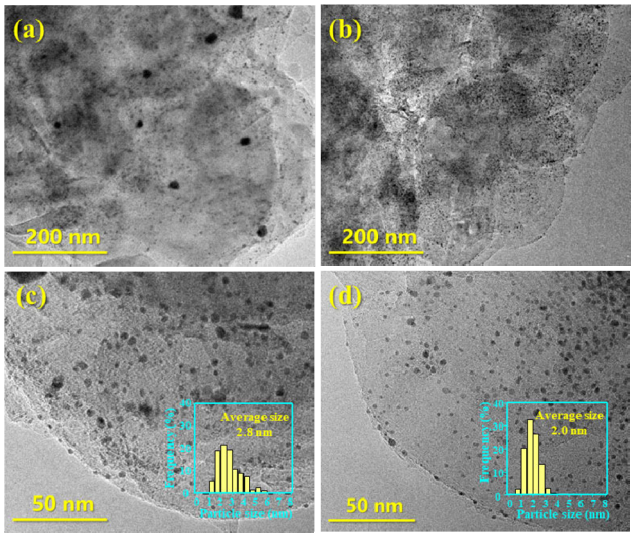

Fig. 1. TEM images and particle-size distributions of Au/BN (a,c) and Au-CuO_x/BN (b,d) catalysts.

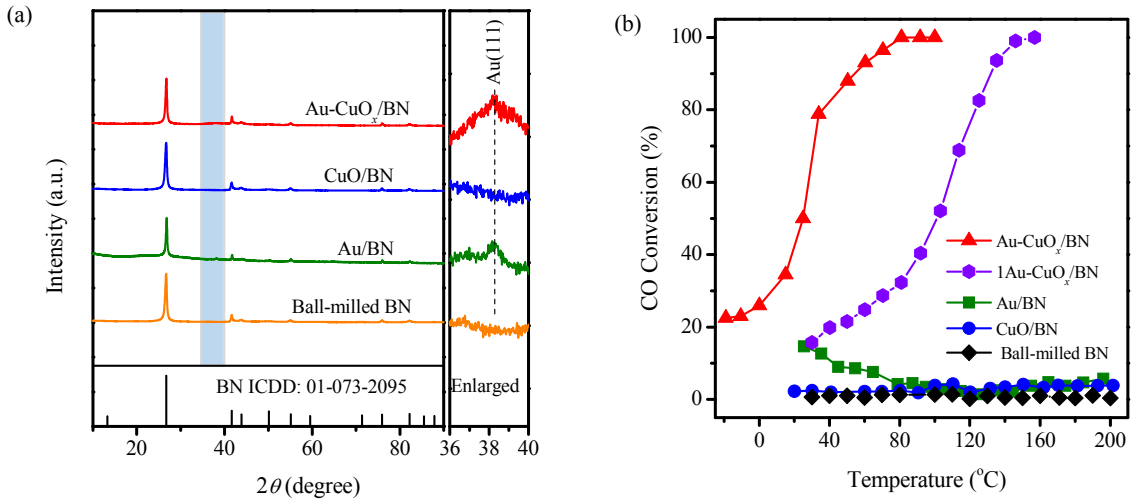

Fig. 2. (a) XRD patterns of ball-milled BN, Au/BN, CuO/BN, and Au-CuO$_x$/BN catalysts; (b) CO oxidation activities of ball-milled BN, CuO/BN, Au/BN, and Au-CuO$_x$/BN catalysts with different Au loadings.

range, CO molecules mainly react with the oxygen species on Au/BN provided by the hydroxyl groups or adsorbed oxygen. An increase in the reaction temperature decreases the coverage of absorbed oxygen-containing surface species and, consequently, lowers catalytic activity [26]. In addition, as shown in Fig. 1(a) and Fig. 3(a), the Au nanoparticles on the Au/BN catalyst are distinctly aggregated after reaction, indicating that *h*-BN does not stabilize Au nanoparticles well. After calcination at 400 °C, the Cu species in the CuO/BN catalyst mainly exist as Cu^{2+} (Fig. 4(c)) that only weakly adsorb CO in the reaction [27]. This leads to poor activity at low temperatures. However, the Au-CuO$_x$/BN catalyst shows excellent CO oxidation activity, with $T_{100\%}$ at 80 °C, which is in the upper level for unreducible supported Au catalysts (Table S2). The high thermal conductivity of BN may be beneficial for reducing the formation of hot spots in the CO oxidation reaction. Furthermore, the functional groups and/or defects on the ball-milled BN may stabilize the CuO, which can then anchor Au species. As a consequence, catalytic activity is improved because of the small immobilized Au particles. When the Au loading is reduced to only 1 wt% (calculated based on a Au/BN mass ratio of 0.01), the 1Au-CuO$_x$/BN catalyst still achieves 100% CO conversion at 150 °C (Fig. 2(b)). Compared to monometallic catalysts, Au-CuO$_x$/BN shows a significant increase in catalytic activity, indicating the promotional effect of Cu species on the BN support.

To identify the origin of the catalytic activity and the effect of Cu addition, a series of structural analyses of the used catalysts was conducted. According to the TEM images, distinct agglomeration of Au particles on the used Au/BN catalysts occurs upon reaction, and the average Au particle size increases to 4.5 nm (Fig. 3(a)). However, in the case of the used Au-CuO$_x$/BN catalyst, the average Au particle size increases only slightly to 2.7 nm (Fig. 3(b)), indicating that the loading of Cu species effectively enhances the stability of Au nanoparticles, keeping them as small as possible (Table S3). The CuO$_x$ may be highly dispersed and stabilized by the –OH and –NH_2 groups over the surface of BN [28], and CuO$_x$ exhibits strong interaction and compatibility with Au. Therefore, the small Au nanoparticles on BN are stabilized with the assistance of CuO$_x$.

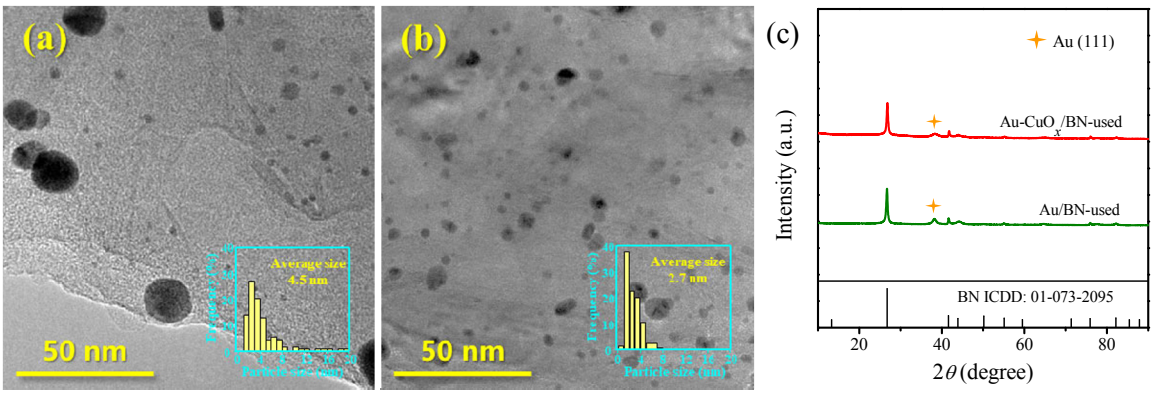

Fig. 3. TEM images and particle size distributions of Au/BN-used (a) and Au-CuO$_x$/BN-used (b) catalysts; (c) XRD patterns of Au/BN-used and Au-CuO$_x$/BN-used catalysts.

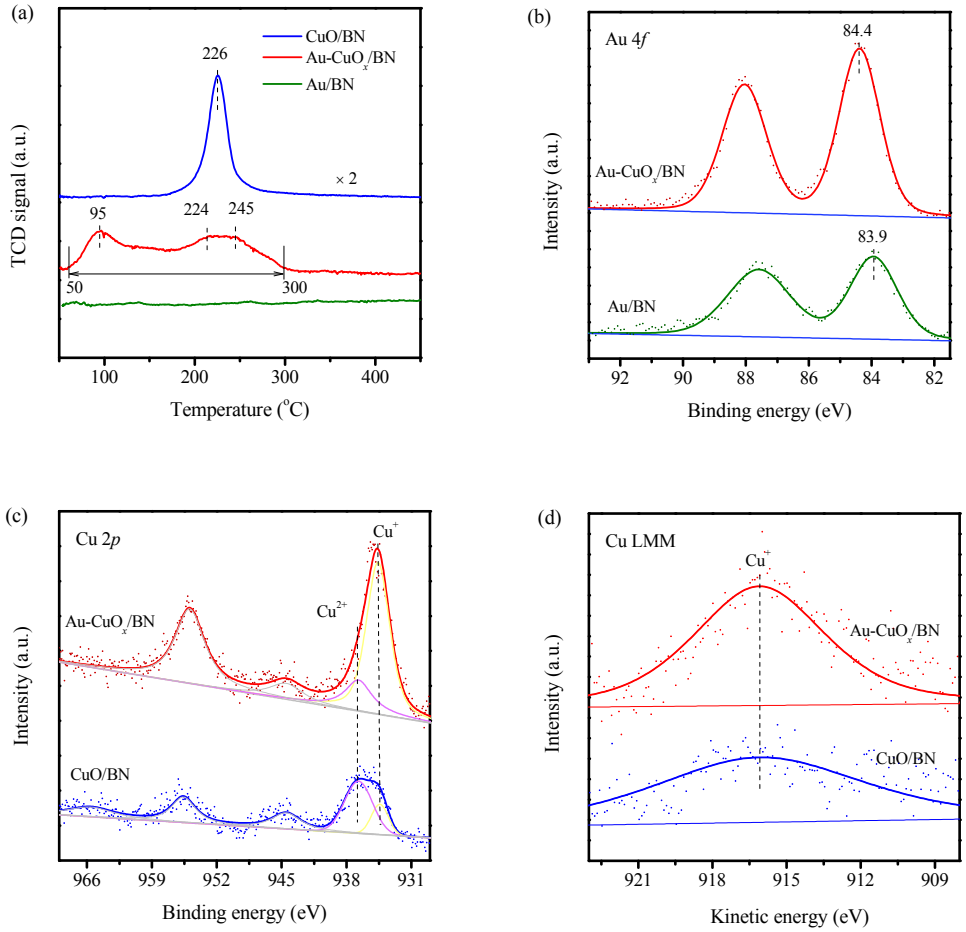

Fig. 4. (a) H_2-TPR patterns of CuO/BN, Au/BN, and Au-CuO_x/BN catalysts; (b) Au 4*f* XPS profiles; Cu 2*p* XPS profiles (c) and corresponding Cu LMM Auger electron spectra (d) of Au-CuO_x/BN and CuO/BN catalysts.

The XRD results show that the intensities of the peaks for Au increase for both used Au/BN and used Au-CuO_x/BN catalysts (Fig. 3(c)), indicating the agglomeration of Au nanoparticles. The results agree with those of TEM observation.

Since the reduction of oxidic Cu and Au species can occur in the CO oxidation reaction, H_2-TPR analysis was performed to study the reduction properties of the catalysts. As shown in Fig. 4(a), no distinct reduction peak is observed for oxidized Au in the Au/BN catalyst, indicating that Au remains in the metallic state after oxidation pretreatment. For the CuO/BN catalyst, the single hydrogen consumption peak at 226 °C is due to the reduction of CuO on the BN support [29]. After depositing Au on CuO/BN, the presence of three reduction peaks instead of one (as in the case of CuO/BN) is an indication of the existence of more than one CuO_x species in the catalyst.

The electronic states of active surface species are crucial factors that influence catalytic behavior. Accordingly, XPS experiments were performed to investigate the local electronic environments of surface Au and Cu species. The photoelectronic splitting of Au in Au/BN results in binding energies of 83.9 and 87.6 eV, assigned respectively to the $4f_{7/2}$ and $4f_{5/2}$ orbitals of metallic Au (Fig. 4(b)) [30]. For Au-CuO_x/BN, both peaks shift to higher binding energies, and this can be attributed to the existence of $Au^{\delta+}$. Furthermore, the corresponding Cu $2p_{3/2}$ spectrum has two peaks, which are assigned to Cu^{2+} and Cu^+ accompanied by characteristic Cu^{2+} shake-up satellite peaks (Fig. 4(c)) [31]. Similarly, both Cu^{2+} and Cu^+ species are detected on the monometallic CuO/BN catalyst. The existence of Cu^+, which has been proved to be beneficial for oxygen activity and mobility, is further confirmed by the Cu LMM Auger spectra (Fig. 4(d)) [32]. Further information can be obtained from the O 1*s* spectra, shown in Fig. S6. For the Au/BN catalyst, the O 1*s* peak centered at 532.9 eV corresponds to oxygen bonded with the B-edge [33]. For the Au-CuO_x/BN catalyst, this peak shifts to a lower binding energy (~531.1 eV), which is due to the existence of lattice oxygen.

CO-DRIFT spectra were obtained to explore the electronic states of the active species (Fig. 5). After CO adsorption saturation, three bands at 2077, 2122, and 2168 cm^{-1} are observed for Au/BN, which may be ascribed to the absorption of CO adsorbed on $Au^{\delta-}$, Au^0, and $Au^{\delta+}$ species, respectively [34–38]. The intensity of the CO absorption peak around 2122 cm^{-1} is higher for Au-CuO_x/BN than for Au/BN owing to the existence of Cu^+ in the former [27,39,40]. The peaks at 2338 and 2360 cm^{-1}

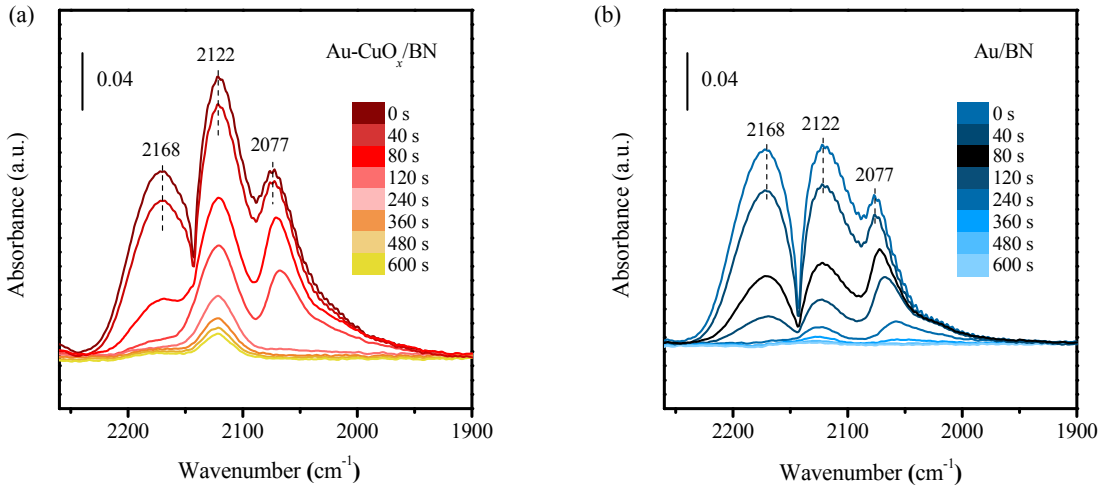

Fig. 5. DRIFT spectra for CO adsorption over Au-CuO$_x$/BN (a) and Au/BN (b) catalysts with nitrogen purging after CO adsorption saturation.

represent gaseous CO_2 over the Au-CuO$_x$/BN catalyst (Fig. S7) [5], and they are not observed for the Au/BN catalyst. This phenomenon may indicate that the activated oxygen on the Au-CuO$_x$/BN catalyst readily reacts with adsorbed CO. It should be pointed out that bands at 2120 and 2170 cm^{-1} are often detected for gaseous CO, which can be easily eliminated by N_2 purging. With increasing purging time, all three bands for the Au/BN catalyst gradually disappear, while the band at 2122 cm^{-1} for Au-CuO$_x$/BN remains. Furthermore, the intensities of the three peaks decrease more slowly for Au-CuO$_x$/BN than for Au/BN upon purging for the same period of time, indicating stronger CO adsorption for the former due to changes in the electronic environments of the Au and Cu species.

Based on these results, the improved catalytic activity of Au-CuO$_x$/BN may be attributed to the electron transfer effects of Au and Cu species. First, the interaction between Au nanoparticles and CuO/BN keeps the size of the Au particles relatively small, thus producing more active sites. Second, CO molecules can be adsorbed on the surfaces of both Au nanoparticles and Cu species, and the introduction of Cu distinctly strengthens CO adsorption on Au-CuO$_x$/BN catalyst. In addition, the changes in the electronic environments of Au and Cu species enhance the mobility of oxygen and thus improve CO oxidation activity at relatively low temperatures over the inert BN support.

4. Conclusions

In this work, ball-milled BN was employed as a catalyst support, upon which Cu species and Au nanoparticles were subsequently loaded. The obtained catalyst showed good performance for CO oxidation with a 100% conversion of CO at 80 °C, which meets the operational temperature requirements for proton exchange membrane fuel cells. On the basis of various characterization results, we deduced that the introduction of Cu promotes the dispersion and stabilization of Au nanoparti-

Graphical Abstract

Chin. J. Catal., 2021, 42: 388–395 doi: 10.1016/S1872-2067(20)63669-5

Highly dispersed boron-nitride/CuO$_x$-supported Au nanoparticles for catalytic CO oxidation at low temperatures

Fan Wu, Lei He, Wen-Cui Li, Rao Lu, Yang Wang, An-Hui Lu *
Dalian University of Technology

Using ball-milled BN as the support, a Au-CuO$_x$/BN catalyst was prepared. This catalyst exhibited high performance in CO oxidation due to the highly dispersed and stabilized Au nanoparticles and strengthened CO adsorption.

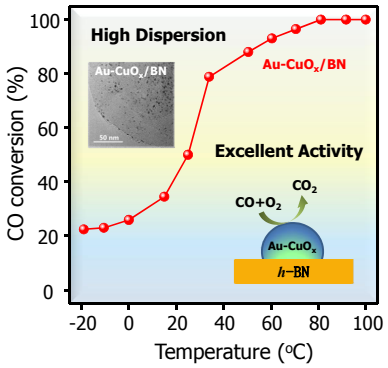

cles on BN, simultaneously strengthening CO adsorption and oxidation. Thus, this study demonstrates a new strategy whereby thermally stable, thermally conductive, and two-dimensionally structured BN can be used as a support material for heterogeneous catalysts.

References

[1] M. Haruta, N. Yamada, T. Kobayashi, S. Iijima, *J. Catal.*, **1989**, 115, 301–309.
[2] A. Stephen, K. Hashmi, G. J. Hutchings, *Angew. Chem. Int. Ed.*, **2006**, 45, 7896–7936.
[3] M. Comotti, W. C. Li, B. Spliethoff, F. Schüth, *J. Am. Chem. Soc.*, **2006**, 128, 917–924.
[4] L. Arab, M. Boutahala, B. Djellouli, T. Dintzer, V. Pitchon, *Appl. Catal. A*, **2014**, 475, 446–460.
[5] T. M. Tran-Thuy, C. C. Chen, S. D. Lin, *ACS Catal.*, **2017**, 7, 4304–4312.
[6] Y. X. Miao, L. Shi, L. N. Cai, W. C. Li, *Gold Bull.*, **2014**, 47, 275–282.
[7] T. Diemant, Z. Zhao, H. Rauscher, J. Bansmann, R. J. Behm, *Surf. Sci.*, **2007**, 601, 3801–3804.
[8] X. Y. Liu, M. H. Liu, Y. C. Luo, C. Y. Mou, S. D. Lin, H. Cheng, J. M. Chen, J. F. Lee, T. S. Lin, *J. Am. Chem. Soc.*, **2012**, 134, 10251–10258.
[9] D. Widmann, R. J. Behm, *Accounts Chem. Res.*, **2014**, 47, 740–749.
[10] D. Widmann, R. J. Behm, *Angew. Chem. Int. Ed.*, **2011**, 50, 10241–10245.
[11] D. A. Bulushev, I. Yuranov, E. I. Suvorova, P. A. Buffat, L. Kiwi-Minsker, *J. Catal.*, **2004**, 224, 8–17.
[12] Y. C. Wang, D. Widmann, R. J. Behm, *ACS Catal.*, **2017**, 7, 2339–2345.
[13] X. S. Huang, H. Sun, L. C. Wang, Y. M. Liu, K. N. Fan, Y. Cao, *Appl. Catal. B*, **2009**, 90, 224–232.
[14] Y. G. Wang, Y. Yoon, V. A. Glezakou, J. Li, R. Rousseau, *J. Am. Chem. Soc.*, **2013**, 135, 10673–10683.
[15] B. L. Moroz, P. A. Pyrjaev, V. I. Zaikovskii, V. I. Bukhtiyarov, *Catal. Today*, **2009**, 144, 292–305.
[16] C. X. Qi, H. J. Su, R. G. Guan, X. F. Xu, *J. Phys. Chem. C*, **2012**, 116, 17492–17500.
[17] R. Lu, L. He, Y. Wang, X. Q. Gao, W. C. Li, *Chin. J. Catal.*, **2020**, 41, 350–356.
[18] Y. X. Miao, J. Wang, W. C. Li, *Chin. J. Catal.*, **2016**, 37, 1721–1728.
[19] J. T. Grant, C. A. Carrero, F. Goeltl, J. Venegas, P. Mueller, S. P. Burt, S. E. Specht, W. P. McDermott, A. Chieregato, I. Hermans, *Science*, **2016**, 354 , 1570–1573.
[20] L. Shi, Y. Wang, B. Yan, W. Song, D. Shao, A. H. Lu, *Chem. Commun.*, **2018**, 54, 10936–10946.
[21] L. Shi, D. Q. Wang, A. H. Lu, *Chin. J. Catal.*, **2018**, 39, 908–913.
[22] Y. Wang, L. Shi, W. D. Lu, Q. Sun, Z. F. Wang, C. Y. Zhi, A. H. Lu, *ChemCatChem*, **2017**, 9, 1363–1367.
[23] X. Y. Sun, M. J. Liu, Y. Y. Huang, B. Li, Z. Zhao, *Chin. J. Catal.*, **2019**, 40, 819–825.
[24] J. J. Luo, Y. F. Liu, Y. M. Niu, Q. Jiang, R. Huang, B. S. Zhang, D. S. Su, *Nanoscale*, **2017**, 9, 15033–15043.
[25] Y. Lin, T. V. Williams, W. Cao, H. E. Elsayed-Ali, J. W. Connell, *J. Phys. Chem. C*, **2010**, 114, 17434–17439
[26] X. J. Xu, Q. Fu, X. G. Guo, X. H. Bao, *ACS Catal.*, **2013**, 3, 1810–1818.
[27] Z. He, H. Q. Lin, P. He, Y. Z. Yuan, *J. Catal.*, **2011**, 277, 54–63.
[28] C. J. Huang, W. Q. Ye, Q. W. Liu, X. Q. Qiu, *ACS Appl. Mater. Interfaces*, **2014**, 6, 14469–14476.
[29] F. C. Duh, D. S. Lee, Y. W. Chen, *Mod. Res. Catal.*, **2013**, 2, 1–8.
[30] H. L. Tang, Y. Su, B. S. Zhang, A. F. Lee, M. A. Isaacs, K. Wilson, L. Li, Y. G. Ren, J. H. Huang, M. Haruta, B. T. Qiao, X. Liu, C. Z. Jin, D. S. Su, J. H. Wang, T. Zhang, *Sci. Adv.*, **2017**, 3, e1700231.
[31] C. X. Qi, Y. H. Zheng, H. Lin, H. J. Su, X. Sun, L. B. Sun, *Appl. Catal. B*, **2019**, 253, 160–169.
[32] T. J. Huang, D. H. Tsai, *Catal. Lett.*, **2003**, 87, 173–178.
[33] L. Shi, D. Q. Wang, W. Song, D. Shao, W. P. Zhang, A. H. Lu, *ChemCatChem*, **2017**, 9, 1788–1793.
[34] A. Hugon, N. E. Kolli, C. Louis, *J. Catal.*, **2010**, 274, 239–250.
[35] A. M. Abdel-Mageed, A. Klyushin, A. Rezvani, A. Knop-Gericke, R. Schlögl, R. Jürgen Behm, *Angew. Chem. Int. Ed.*, **2019**, 58, 10325–10329.
[36] T. Venkov, K. Fajerwerg, L. Delannoy, H. Klimev, K. Hadjiivanov, C. Louis, *Appl. Catal. A*, **2006**, 301, 106–114.
[37] T. Venkov, H. Klimev, M. A. Centeno, J. A. Odriozola, K. Hadjiivanov, *Catal. Commun.*, **2006**, 7, 308–313.
[38] F. Romero-Sarria, A. Penkova, L. M. T. Martinez, M. A. Centeno, K. Hadjiivanov, J. A. Odriozola, *Appl. Catal. B*, **2008**, 84, 119–124.
[39] W. Z. Yu, W. W. Wang, S. Q. Li, X. P. Fu, X. Wang, K. Wu, R. Si, C. Ma, C. J. Jia, C. H. Yan, *J. Am. Chem. Soc.*, **2019**, 141, 17548–17557.
[40] X. Y. Liu, A. Q. Wang, L. Li, T. Zhang, C. Y. Mou, J. F. Lee, *J. Catal.*, **2011**, 278, 288–296.

氮化硼负载的高分散Au-CuO_x纳米颗粒用于低温CO氧化

吴 凡, 贺 雷, 李文翠, 路 饶, 王 阳, 陆安慧*

大连理工大学化工学院, 精细化工国家重点实验室, 辽宁省低碳资源高值化利用重点实验室, 辽宁大连 116024

摘要: 负载型金催化剂显示出高的低温CO氧化活性, 其催化性能与载体的性质密切相关. 近年来, 六方氮化硼作为一种新型催化材料引起了极大关注. 已有研究表明, 二维结构的氮化硼纳米片有利于传质扩散, 并且暴露出大量的表面和边缘, 作为新型非金属催化剂在烷烃氧化脱氢中表现出优异的活性. 同时, CO氧化反应是强放热过程, 氮化硼具有优良的导热性能, 能够减少反应过程中热点的形成. 然而氮化硼是非还原性载体, 与活性组分金之间的相互作用较弱, 需要通过改性来加强金与氮化硼载体间的相互作用.

基于此, 本文首先通过球磨处理来获得具有高比表面积和富缺陷的氮化硼纳米片载体, 采用浸渍法在氮化硼纳米片上引入铜物种, 实现对载体的改性, 然后采用传统的沉积-沉淀法制备Au-CuO_x/BN催化剂. 经氧化性气氛预处理后, Au-CuO_x/BN催化剂表现出良好的低温CO氧化活性, 80 °C下即可实现CO的完全转化.

采用X射线衍射(XRD), 高分辨透射电镜(HRTEM), 氢气程序升温还原(H_2-TPR), X射线光电子能谱(XPS), CO吸附原位

漫反射红外光谱(CO-DRIFT)等表征手段深入分析了Au-CuO_x/BN的结构与催化活性的关系. XRD测试结果未观察到明显的金和铜物种衍射峰, 表明二者在氮化硼载体上高度分散. HRTEM和元素分析面扫描结果进一步表明, 氧化铜主要分布于BN边缘的官能团和缺陷位上, 金纳米粒子与铜物种的空间分布位置一致, 表明BN通过稳定CuO_x物种进而实现了金纳米粒子(2.0 nm)的高分散, 且反应后的金纳米粒子未发生明显团聚. H_2-TPR结果表明金和铜物种间的相互作用可促进铜物种的还原, XPS分析进一步证实了金和铜物种之间存在电子转移. CO-DRIFT结果表明, Au-CuO_x/BN催化剂对CO的吸附能力和提供活性氧物种的能力显著强于Au/BN催化剂, 从而促进了CO氧化反应. 综上, 铜物种作为连接金和氮化硼载体之间的桥梁, 促进了金纳米粒子在氮化硼载体上的分散和稳定, 同时增强了CO的吸附和氧的活化. 本文拓展了氮化硼在多相催化中的应用, 为发展新型二维催化材料提供新的思路.

关键词: 氮化硼; 金催化剂; 一氧化碳氧化; 氧化铜; 电子转移

收稿日期: 2020-04-20. 接受日期: 2020-05-26. 出版日期: 2021-03-05.

*通讯联系人. 电话: (0411) 84986112; 电子信箱: anhuilu@dlut.edu.cn

基金来源: 国家自然科学基金(21733002); 中德联合研究计划(21761132011); 中国长江学者计划(T2015036).
本文的电子版全文由Elsevier出版社在ScienceDirect上出版(http://www.sciencedirect.com/science/journal/18722067).